Check for updates

Review

International Journal of
Protective Structures

Blast wave ingress into a room through an opening – Review of past research and US DoD UFC 3-340-02

International Journal of Protective Structures
2024, Vol. 0(0) 1–24
© The Author(s) 2024

Article reuse guidelines:
sagepub.com/journals-permissions
DOI: 10.1177/20414196241277222
journals.sagepub.com/home/prs

Alex Eytan[1], Shaun A Forth[1], Erik G Pickering[2], Rachael Hazael[2] and Stephanie J Burrows[1]

Abstract

Blast wave ingress into a room through a facade opening results in complex pressure-time loadings on interior surfaces due to shock diffraction and interior reflections. The U.S. DoD UFC 3-340-02 *Structures to Resist the Effects of Accidental Explosions* includes a method to predict internal loading for such cases. Parameters such as the opening size, room dimensions and the external pressure wave characteristics influence the interior loading. Recent work suggests that the UFC methodology might overpredict the interior loading by some 600%. Such conservatism can result in over-engineered or prohibitively expensive protective solutions. In this paper we critically review the methodology of the UFC, that of Kaplan's preceding work (on which the UFC relies), and the experimental data that informed both these works. Through a series of 45 case-studies we compare the UFC and Kaplan's predictions with those of a computational fluid dynamics (CFD) model. The UFC consistently overpredicts the CFD area-averaged peak pressure of the back wall by up to 290% and the side-wall by up to 425%. Similarly, the UFC overpredicted the CFD side wall positive phase impulse by up to 565%. By contrast, the UFC predicted back wall positive phase impulse was similar to the CFD results. As our CFD results for side and back walls are area averaged, and not solely for the wall centre-point, as in other recent work, our paper gives support for the use of CFD prediction over the UFC for cost-effective design of structures to resist blast ingress.

Keywords

UFC 3-340-02, blast ingress, blast leakage, interior wall loading, blast modelling

[1]Cranfield Defence and Security, Cranfield University, Defence Academy of the United Kingdom, Shrivenham, UK
[2]Cranfield Forensic Institute, Cranfield University, Defence Academy of the United Kingdom, Shrivenham, UK

Corresponding author:
Alex Eytan, Centre for Systems, Simulation & Analytics, Cranfield University, Defence Academy of the United Kingdom, Shrivenham SN6 8LA, UK.
Email: alex.eytan@cranfield.ac.uk

Introduction

The facade of a structure at known risk of blast loading is usually designed to reflect the oncoming shock wave. In many cases the shock can "leak" or ingress into the structure through necessary facade openings. The shock propagates through the interior by a complex sequence of diffractions and reflections with the interior loading dependent on the structure's geometry. This complicates the task of designing blast resistant interior walls, floors and ceilings. A commonly employed methodology for predicting loads from blast ingress is Section 2-15.4 of UFC 3-340-02 Structures to Resist the Effects of Accidental Explosions (U.S. Department of Defense, 2014), hereafter referred to as the UFC.

There are three typical cases where blast ingress consideration should occur as part of the design of protective structures. The first occurs in countries with increased terrorism risk, where government and business resilience is actively increased by providing blast protection to critical buildings. When protecting the entire building is infeasible, safe havens may be provided inside the structure. Such protected spaces are provided in all newly built public and commercial buildings in both Singapore (Singapore Civil Defence Shelter Act, 1997) and Israel (IDF HFC, 2010), as well as in embassies worldwide. In such instances, the shock is likely to ingress through failed parts of the unprotected facade, or through open windows or doors, and then load the safe haven's walls.

The second case results from the ventilation required for occupants and operations. In protected critical infrastructure, such as command rooms and data centres, there is an increased demand for high flow air intake for backup generators and cooling equipment (U.S. FEMA, 2006). To prevent blast leakage, a pressure valve (U.S. Army Corps of Engineers, 2009) is fitted to all air intake ducts. As most such valves do not support high flow rates, numerous valves are needed which may both complicate the design and require an increase in the structure's exposed face area, as seen in Figure 1.

Finally, any protected facade that includes a doorway should consider the effects of shock ingress through a door left open during an attack. This case is often neglected in blast vulnerability analysis.

Within the open literature there is minimal research published on the topic of blast ingress. Amongst the earliest publications was a method to calculate the pressure change inside a room as a result of leakage through a small opening which was published in 1962 (BRL, 1962). It was incorporated into the first edition of the "TM 5-1300 - Structures to Resist the Effects of Accidental Explosions" manual (US Department of Commerce, 1969). Kaplan (1979) developed a method to



Figure 1. An array of circular blast valves in an external civil defence shelter wall, Helsinki, Finland (Image courtesy of Temet International Oy Ltd).

predict the loading on interior walls which formed the basis for a future method, and is reviewed in detail hereafter. Kingery and Watson (1982) reported research on pressure leakage into hardened aircraft shelters through an open door and included a comparison with Kaplan's (1979) method. It suggested that Kaplan's method overpredicts the interior pressure for cases of narrow openings but might be adequate for large openings. Ayvazyan et al. (1986) produced an extension to TM 5-1300 chapter four (US Department of Commerce, 1969) to include a new method for predicting pressure and impulse on interior walls from shock ingress. Their method was incorporated into the updated TM 5-1300 (U.S. Department of Defense, 1990). In the early 1990s, shock tube experiments on pressure ingress were performed by Mercx (1990a, 1990b, 1991), which resulted in a calculation method produced by curve fitting functions for a limited set of room sizes.

In related work, Feldgun et al. (2016) and Xu et al. (2018) considered pressure leakage outwards from a partially confined explosion but focused on the quasi-static loading from afterburning effects. Within a cityscape it has been shown that pressure ingress from failed facades result in reduced risk for neighbouring buildings (Drazin, 2017; Smith et al., 2002) and increased risk for supposedly shielded buildings (Dib et al., 2022).

For complex internal structures, Ram et al.'s (2016) study of interior partitioning effects on pressure ingress suggested that interior loading develops in a similar manner to that of shock transmission through porous materials. The shock attenuation properties of porous/lattice geometries were reported by Abdelaim (2013), Berger et al. (2015), Britan et al. (2006) and Skews (2005). They demonstrated how different geometric obstacles manipulate the shock gas flow and drew a relationship between porosity and rearward pressure.

In work directly relevant to ours, Codina and Ambrosini (2018, 2019) conducted a limited set of full-scale experiments of blast ingress into a cuboid structure and compared the results from their four blast gauges with the corresponding UFC predictions. They concluded the UFC underestimates the impulse on the back wall by up to 60% and overestimates it on the side wall by up to 685%. They proposed correction factors to the UFC to better match their experimental data.

The UFC's purpose is to serve as a manual for safe design of structures at risk of blast loading and therefore is expected to be conservative. Most standards apply a safety factor in their calculations to account for variability in design parameters. Indeed, the UFC itself recommends applying a 20% increase to the charge mass as part of the design process. However, conservatism in excess of 600% as reported by Codina and Ambrosini (2018, 2019) is beyond practical safe design principles and causes us to question the UFC's underlying theory for blast ingress.

Within his work that underpinned the UFC, Kaplan (1979) repeatedly asserts the need for further testing and assessment of his methodology which was developed by limited experimental data. Despite the three reissues of the UFC (1990, 2008, 2014) we can find no reports of such work being performed. As such we have undertaken a review of the theory and data used in the UFC. This work is hampered because the UFC, as a technical manual, presents graphs of predicted loading without detailing how these graphs were derived.

Other blast resistance design standards (ASCE 59-11, 2011; CSA S850-12, 2012) acknowledge proper computational modelling (or indeed, physical testing) is a valid method to assess blast loading and response. Such tools were not widely available at the time blast ingress was incorporated into the UFC.

In this paper, we present and review Kaplan's (1979) methodology on which the UFC appears to be based. We outline the current UFC approach, highlighting several issues we believe require addressing. Thereafter we compare the results from these two calculation methods with an appropriate CFD model. Our conclusions and description of future work are then summarised.

Kaplan's 1979 model

Kaplan (1979) (referred to as Kaplan henceforth) details a method for predicting internal loading from blast ingress dependent on the room dimensions (width W, height H and length L), facade area $A_f = H \times W$, facade opening area A_o, external pressure wave characteristics (peak facade overpressure P_{SO} and standoff distance from the charge d) and ambient pressure P_0. Kaplan's methodology was derived and validated against results from three test series:

(1) A 2.4 × 2.4 × 3.6 m concrete cubicle, with a 2.1 × 0.88 m opening subjected to an incident peak pressure of 32.4 kPa and 200 msec duration from a 500,000 kg hemispherical TNT charge.
(2) Shock tube tests simulating a scaled 500,000 kg hemispherical TNT charge with duration of 160 msec using a 1:24 scale structure (Coulter, 1969).
(3) Shock tube tests on a full-scale room with a 2.6 × 3.6 m facade subjected to peak pressure of 69 kPa and 100 msec duration (Wilton et al., 1978).

Kaplan defined a relative opening area $A_r = \frac{A_0}{A_w}$, an effective facade opening diameter $b_O = \sqrt{4A_0/\pi}$, and considered the interior shock evolution with distance d' from the opening as depicted in Figure 2. Kaplan suggested that the wave behaviour downstream from the opening can be separated into three different phases.

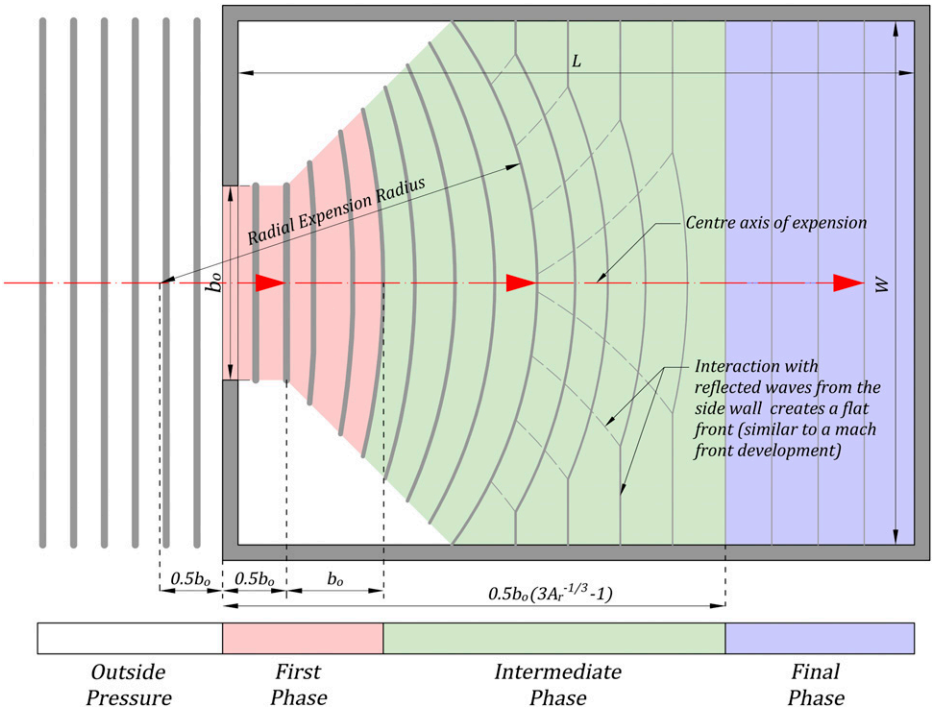


Figure 2. Plan view of Kaplan's (1979) proposed three phases of interior shock wave development as a function of the distance d' travelled from the opening relative to the opening's effective diameter b_0 and relative to the total facade area A_r.

(1) First Phase – the shock is assumed to be initially planar and remains so until $d' = 0.5b_o$. Then, as the shock wave diffracts from the opening edge it widens and its front curves, while the central area remains near planar.
(2) Intermediate Phase – at $d' = 1.5b_o$, the entire shock front is assumed curved and diffracts further until it reflects off the side walls, ceiling or floor.
(3) Final Phase – it is assumed that multiple reflections from the sidewall, ceiling and/or the floor in the Intermediate Phase have caused the shock to become planar again before it reaches the rear wall. Kaplan states that while "…*it is difficult to say when it* [the planar wave] *can be said to form…a reasonable (though still arbitrary) guideline*" is at a distance $d_l' = 0.75b_O\,(3A_r^{-1/3} - 1)$, where the pressure along the wave sides is equal to the pressure along the centre axis.

Calculating the pressure along the centre axis

Kaplan calculates the shock front pressure $P_s(d')$ along the facade centre axis as follows):

$$\text{For } 0 \le d'/b_O \le 1/2, \qquad \frac{P_S}{P_{SO}} = [1+(d'/d)]^{-1.5} \tag{2-1}$$

$$\text{For } 1/2 < d'/b_O \le 3/2, \qquad \frac{P_S}{P_{SO}} = 0.75\left(\frac{d'}{b_0}\right)^{-0.4} \cdot [1 + (d'/d)]^{-1.5} \tag{2-2}$$

$$\text{For } 3/2 < d'/b_O \le d_l'/b_O, \qquad \frac{P_S}{P_{SO}} = \left[\frac{(2d' + b_O)}{3b_O}\right]^{-3.2} \cdot [1+(d'/d)]^{-1.5} \tag{2-3}$$

$$\text{For } d_l'/b_O < d'/b_O, \qquad \frac{P_S}{P_{SO}} = (A_r)^{0.5} \cdot [1+(d'/d)]^{-1.5} \tag{2-4}$$

In Equation 2-1, 2-2, 2-3 and 2-4, the factor $[1 + (d'/d)]^{-1.5}$ accounts for the spherical expansion of the shock at small scaled distances.

Calculating the off-axis pressure

In Kaplan's model, the shock front's off-axis pressure $P_{S\theta}(d', \theta)$ is a function of the on-axis pressure $P_s(d')$ and, "…*in the absence of a detailed analysis*", a linear dependence on θ (in degrees), the angle from the centre axis as per Figure 3, is assumed such that:

$$P_{S\theta} = P_S(90° - \theta)/90° \tag{2-5}$$

$$\tan\theta = y/[x + (b_O/2)] \tag{2-6}$$

The side wall reflected pressure P_{sr} is dependent on the shock front pressure P_S, the shock's incident angle on the wall $(90° - \theta)$ and the reflected pressure coefficient. Kaplan considered coefficient formulae from TM 5-1300 (US Department of Commerce, 1969) and Glasstone (1964), but preferred his own simpler forms:

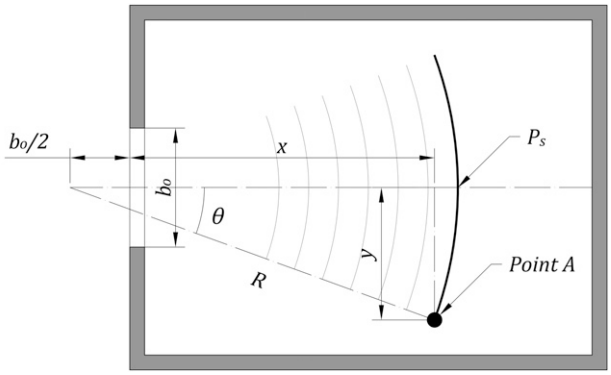


Figure 3. Plan view illustrating the parameters to calculate the off-axis pressure $P_{S\theta}$ at point A as per Equations (2-5) and (2-6).

$$\text{for } 0° \leq \theta \leq 20°, \qquad P_{sr} = P_s \left[\frac{\theta}{10°}\right] \left[\frac{90° - \theta}{90°}\right] \tag{2-7}$$

$$\text{for } \theta > 20°, \qquad P_{sr} = 2P_s \left[\frac{90° - \theta}{90°}\right] \tag{2-8}$$

Kaplan suggested that when the shock expands from the opening there are "…*uncertainties about the value of pressure*" reaching the wall, whether it is incident or reflective, and that the "*shock front itself might not be too well defined*".

If the shock reaches the rear wall during the intermediate phase, the reflected pressure is calculated as per Glasstone's (1964) formula,

$$P_{sr} = \frac{2P_{S\theta}(7P_O + 4P_{S\theta})}{(7P_O + P_{S\theta})} \tag{2-9}$$

Shock reflections from the rear wall may be re-reflected at the front wall, reduced by partial outward venting, to give the re-reflected pressure $P_{sp'}$, where

$$P_{sp'} = P_s \left[1 - \frac{A_o}{A_w}\right] \tag{2-10}$$

Such interior reflections can repeat for "…*several such cycles*" (Kaplan, 1979).

Calculating the pressure-time history on interior walls

For design purposes, Kaplan concludes that the Final Phase pressure Equation (2-4) should be used for both side and rear wall loading irrespective of the shock theory previously described. Kaplan reasoned that the actual "…*pressures themselves could be both greater and smaller than plane wave values*…", and the planar wave is rather "*in the middle*". Kaplan adopted TM 5-1300's (US Department of Commerce, 1969) equivalent uniform pressure loading profiles of Figure 4 for the side wall and Figure 5 for the back wall.

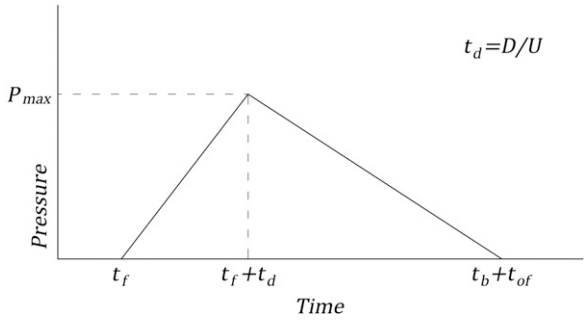


Figure 4. TM 5-1300 – Equivalent uniform pressure loading for a Side Wall span perpendicular to the shock plane, with t_f the wall's shock arrival time, $t_d = D/U$ the resulting time interval to maximum pressure (D the distance the shock exacts maximum stress, U is the shock velocity), t_b the shock arrival time to the end of the wall, $t_{of} = 2i_s/P_{so}$ and i_s the incident impulse at the facade.

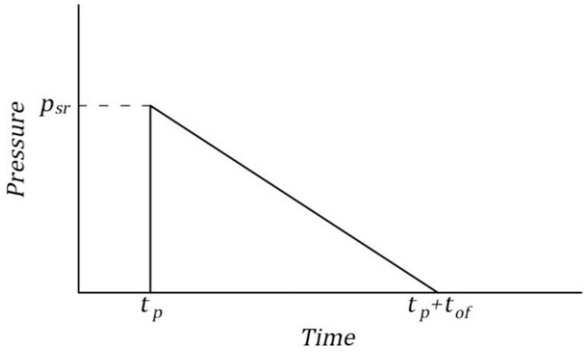


Figure 5. Kaplan's (1979) equivalent uniform pressure loading for the rear wall for instantaneous peak reflected pressure P_{sr} Equation (2-9) and arrival time t_p.

Kaplan states that the methodology is valid for "…*structures located where initial peak blast overpressures from accidental explosions range from about 1 psi* [6.9 kPa] *to 20 psi* [137.9 kPa]*"*. Kaplan defines accidental explosions as those fitting Brode's (1957) pressure-time relationship, that is the Friedlander equation (Friedlander, 1946). Out of 21 experiments examined by Kaplan, 20 were shock tube experiments with a non-Friedlander pressure curve. Furthermore, out of the 21 experiments 80% were performed in the 31.0-41.4 kPa range, with the remaining 20% at ranges of 6.9-73.8 kPa. It is therefore unclear how Kaplan claims validation for overpressures up to 137.9 kPa, and how the UFC extends the range to 296.5 kPa.

Acknowledged limitations

Kaplan acknowledges the limitations of his method stating that "*inadequate data exists on some important blast phenomena that are size dependent.*". As such he concludes with a recommendation to "…*design and carry out an analytical and experimental program involving blast waves that are relatively short compared with structural dimensions"*. To the authors' knowledge none of this recommended work has been performed to date.

The UFC 3-340-02 method

The purpose of the UFC is to provide "easy to use" predictive tools. It provides graphical solutions for typical structure sizes using shock parameters such as incident overpressure P_{SO} and the wavelength of the incident blast wave L_W. The UFC includes paragraphs taken verbatim from Kaplan (1979), and acknowledges both Kaplan and the experimental data it uses (Coulter, 1968, 1969; Wilton et al., 1978). It does not include any other references regarding its blast ingress methodology. Whilst it references these preceding publications, it uses a different idealised pressure-time history for the side wall, as depicted in Figure 6.

The functional dependence of the times $T_1 - T_4$ depicted in Figure 6 is summarised in Table 1 along with the values of the small number of ratios of W/H, L/H and L_W/H for which the UFC supplies blast parameters. For intermediate ratios of these parameters the UFC suggests the use of interpolation. The maximum pressure P_{max} is given by:

$$P_{max} = \frac{K}{(L_W/L)} \tag{3-1}$$

$$\text{For } 1.5 \le W/H \le 6,\ K = \left\{A + \left[B \cdot (L_W/L)^C\right]\right\} \cdot D \cdot E \cdot P_{SO}{}^{1.025} \tag{3-2}$$

$$\text{For } W/H = 0.75,\ K = A \cdot B \cdot C^E \cdot F^H \cdot P_{SO}{}^{0.9718} \tag{3-3}$$

with parameters A-H as defined in Appendix B. As per Figure 6, the impulse is given by

$$I = \frac{P_{max}}{2}\left[(T_4 - T_1) + (T_3 - T_2)\right] \tag{3-4}$$

The form of the back wall parameters $\boldsymbol{P_{RIB}}$, $\boldsymbol{T_1}$ and $\boldsymbol{T_2}$ of Figure 7 are summarised in Table 2, with the impulse given by Equation 3-5

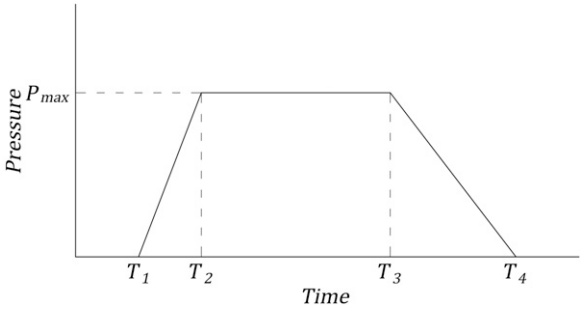


Figure 6. Idealised side wall loading used by the UFC 3-340-02 defined by the four time points ($\boldsymbol{T_1}$, $\boldsymbol{T_2}$, $\boldsymbol{T_3}$, $\boldsymbol{T_4}$) and maximum plateau pressure $\boldsymbol{P_{max}}$.

Table 1. UFC Side Wall $\boldsymbol{T_{1:4}}$ Parameters Dependency.

For	$T_{1:2} = f\left(P_{SO}, \frac{W}{H}\right)$	$T_{3:4} = f\left(P_{SO}, \frac{W}{H}, \frac{L}{H}, \frac{L_w}{L}\right)$
Where	$7 \le P_{SO} \le 220$ kPa	$7 \le P_{SO} \le 220$ kPa
Geometric parameter ratios	$\frac{W}{H} = \frac{3}{4}, \frac{3}{2}, 3, 6$	$\frac{W}{H} = \frac{3}{4}, \frac{3}{2}, 3, 6$ $\frac{L}{H} = 1, 2, 4, 8$ $\frac{L_W}{L} = \frac{3}{8}, \frac{1}{2}, \frac{3}{4}, 1, \frac{3}{2}, 2$

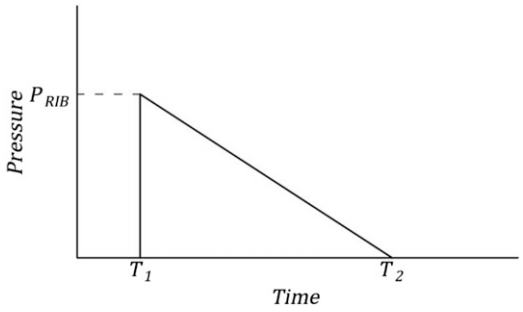


Figure 7. UFC 3-340-02 – Idealised back wall loading defined by two time points T_1, T_2, and instantaneous peak reflected pressure P_{RIB}.

Table 2. UFC Back Wall P_{RIB}, T_1 and T_2 Parameters Dependency.

For	$P_{RIB} = f\left(P_{SO}, \frac{L}{H}, \frac{A_O}{A_W}\right)$	$T_1 = f\left(P_{SO}, \frac{W}{H}, \frac{L}{H}, \frac{A_O}{A_W}\right)$	$T_{3:4} = f\left(P_{SO}, \frac{A_O}{A_W}, W^{1/3}\right)$
Where		$14 \le P_{SO} \le 220$ psi , $\frac{A_O}{A_W} = \frac{1}{8}, \frac{3}{16}, \frac{1}{4}, \frac{3}{8}, \frac{1}{2}$	
Geometric parameter ratios	$L/H = 1, 2, 4, 8$	$\frac{W}{H} = \frac{3}{4}, \frac{3}{2}, 3, 6$	$\frac{L}{H} = 1, 2, 4, 8$ $W_{TNT}{}^{(1/3)}$

$$I = \frac{P_{RIB}}{2}(T_2 - T_1) \tag{3-5}$$

With the UFC methodology thus laid out and contrasted to that of its most likely basis Kaplan (1979), careful analysis of the UFC raises concerns over its reliability. These are discussed in the subsequent sections as per the order they appear in the UFC.

Side wall maximum pressure P_{max}

To better illustrate the sensitivity of the side wall maximum pressure P_{max} to the geometric parameters (W/H; $L/H, A_O/A_W$), we consider a simplified form of Equation (3-2) and (3-3) in which both P_{SO} exponents, 1.025 and 0.9718, are set to 1. The resulting error from this simplification is less than 10% for the parameter ranges explored. This allows us to plot the simplified P_{max}/P_{SO} as a function of L_w/L in Figure 8 for four sets of geometric parameters.

From Figure 8(a), for $A_o/A_w = 0.25$ and $L/H = 1$ the UFC side wall peak relative pressure P_{max}/P_{SO} consistently increases with relative shock wavelength L_w/L for all relative widths W/H. However, for $W/H = 0.75$ in the other graphs of Figure 8, P_{max} either increases more rapidly with L_w/L than for the other W/H ratios or behaves non-monotonically. It is unclear if this behaviour is intentional and reflects a behaviour that its authors were aware of. Furthermore, interpolation is suggested for values between $W/H = 0.75$ and $/H = 1.5$, as such it is not a single outlier curve but will influence side wall pressure calculations for a range of narrow rooms/corridors.

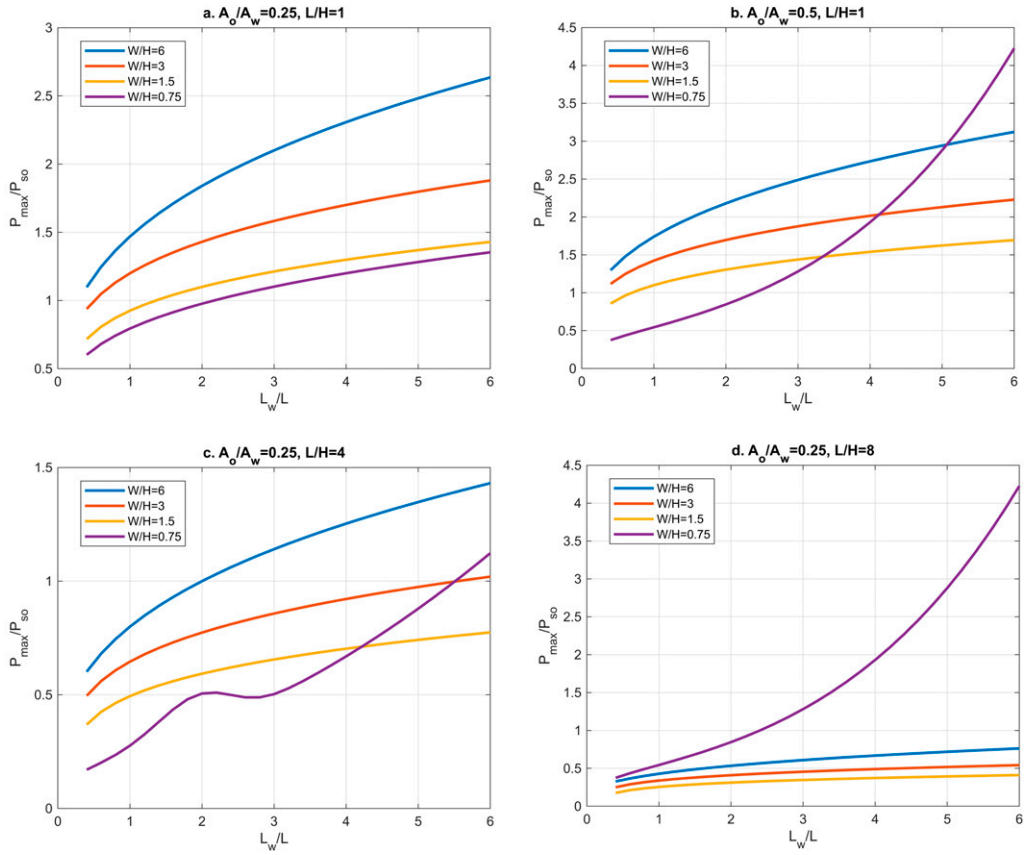


Figure 8. (a-d) Variation of the simplified UFC side wall pressure ratio P_{max}/P_{SO} with shock relative wavelength L_w/L for different opening ratios A_0/A_w and building aspect ratios.

Side wall pressure times T_1, T_2, T_3 and T_4

The side wall impulse is a function of the four side wall timings as shown by Figure 6. Firstly, it is important to note that the UFC determines T_1 and T_2 using the incident pressure P_{so} and the front face aspect ratio W/H but not the cubicle's physical width W or height H. Consequently, cubicles with different physical widths W or heights H under the same shock loading will have the same T_1 and T_2 despite the shock travelling a different distance at the same shock speed.

Secondly, the UFC does not use the side wall length L nor the relative wavelength L_W/L in determining T_2.

Thirdly, consider the UFC solutions for the end time of the maximal positive loading T_4. Figure 9 plots T_4 against P_{SO} for $L/H = 2$ and $W/H = \frac{3}{2}$, we observe that for $P_{SO} = 7$ to 40 kPa, T_4 sharply decreases with P_{SO}, but then for $P_{SO} \gtrsim 40$ kPa it gradually increases. This same behaviour observed is replicated for other building ratios. Consider a single sized structure subjected to different pressures P_{SO} for varying shock wavelength $\frac{L_w}{L}$. The difference in T_4 might be attributed to the change in shock velocity, but this is seen (broken line) in Figure 9 to have a near linear increase with P_{SO}. The UFC's non-monotonic behaviour for T_4 with P_{SO} therefore appears problematic.

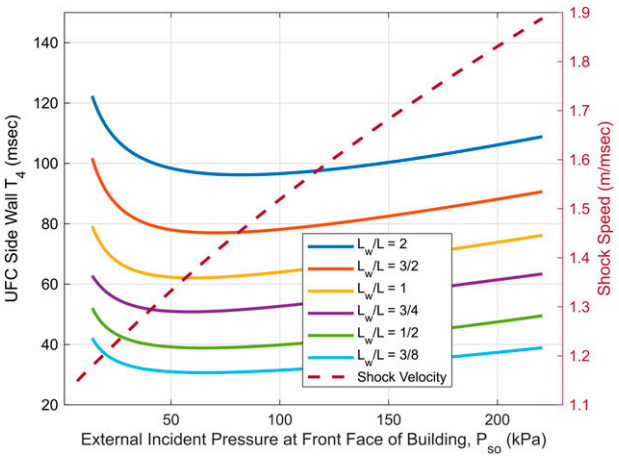


Figure 9. The UFC loading duration T_4 (left-hand axis) and shock speed (dashed, right hand axis) for a side wall with $W/H = 3/2$, $L/H = 2$ versus external incident pressure for various L_w/L ratios.

Back wall time of arrival T_1

The UFC's back wall time of arrival T_1 is dependent on the building aspect ratio W/H. Our analysis (see Appendix C) suggests that the UFC calculates T_1 as the time taken for the shock to reach the back wall corner (Point A in Figure Apx C-1), rather than its centre (the shortest distance). As such, it might not consider the loading occurring between time T_1' when the shock reaches the centre of the wall and T_1 (as depicted in Figure Apx C-1). In cases where the back wall is relatively wide, this might result in a considerable underestimate of impulse.

Back wall positive phase duration

In line with Kaplan, the UFC does not consider the effect of the building length on the positive phase loading duration. By contrast, Kaplan's approach explicitly accounts for the re-reflected shock from the interior front wall whilst it is unclear if the UFC's single triangular pulse of Figure 7 accounts for any interior reflections.

Comparative example of loading methods

To better understand the relationship between Kaplan (1979), the UFC and their potential errors, a CFD comparison was performed for 45 cases of a cuboid structure. Dimensions were chosen to represent a typical small room, with $W/H = \frac{3}{2}, \frac{3}{4}$, $L/H = 1$, opening ratio $A_o/A_w = \frac{3}{16}, \frac{1}{2}$ and $L_w/L = \frac{1}{2}, 2$ so as to match the UFC solutions without the requirement for interpolation. The cases considered are grouped into series, with each series comprising of five incident pressures labelled A to E of 34, 69, 103, 138 and 172 kPa (5,10,15,20,25 psi), respectively, as detailed in Table 3. An example of the typical structure of Series 1 and 2 is depicted in Figure 10. The blast parameters and building dimensions for each case are detailed in Appendix A.

Table 3. Comparative Example Cases Parameters.

Series no.	Cases	W/H	L/H	A_o/A_w	L_w/L
Series 1	1A, 1B, 1C, 1D, 1E	3/2	1	3/16	1/2
Series 2	2A, 2B, 2C, 2D, 2E	3/2	1	1/2	1/2
Series 3	3A, 3B, 3C, 3D, 3E	3/2	1	3/16	2
Series 4	4A, 4B, 4C, 4D, 4E	3/2	1	1/2	2
Series 5	5A, 5B, 5C, 5D, 5E	3/4	1	3/16	1/2
Series 6	6A, 6B, 6C, 6D, 6E	3/4	1	1/2	1/2
Series 7	7A, 7B, 7C, 7D, 7E	3/4	1	3/16	2
Series 8	8A, 8B, 8C, 8D, 8E	3/4	1	1/2	2
Series 9	9A, 9B, 9C, 9D, 9E	3/4	1	1/2	4

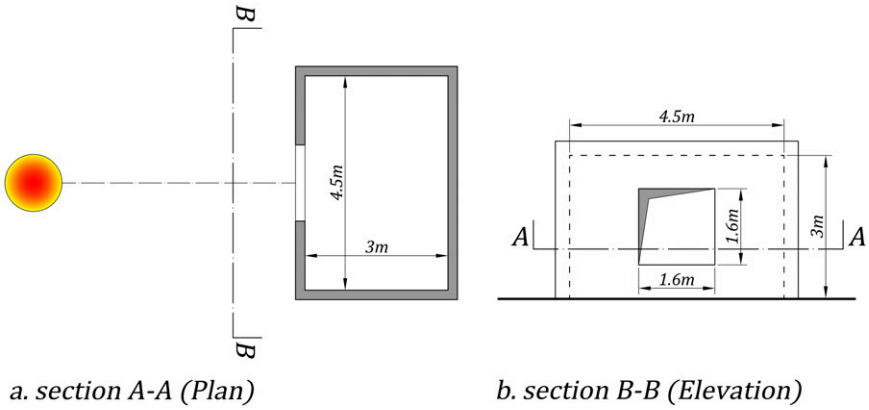


Figure 10. Dimensions of the cuboid structure of Series 1 and 3 with $\boldsymbol{W/H = \frac{3}{2}}$, $\boldsymbol{A_o/A_w = \frac{3}{16}}$

CFD solutions were produced using the computational blast loading tool ProSAir (Forth, 2022) with the simulation parameters detailed in Appendix D. The blast loading was modelled in three stages to exploit the symmetry conditions. In the first stage the loading was modelled as an ideal spherical charge at 1.5 m above ground (structure mid-height) for a 1.5 m radius spherically symmetric domain until the blast wave reached the ground. This spherical model used a mesh size equal to one fiftieth the charge radius as per the ProSAir user manual. The results were then remapped to a 2D axisymmetric domain with a perfectly reflective base to represent the ground and a mesh size of 5 mm. When the pressure wave reached a radius equal to the standoff distance for each case, the model was remapped to a 3D domain. The building was modelled using half-symmetry to exploit the reflective-symmetry across the building centre-axis, using a 50 mm mesh cell size which was sufficiently small to accurately capture the shock pressures. The pressure was recorded on a grid of 100 mm spacing on the side and back walls.

Whilst the UFC and Kaplan methods provide a single equivalent uniform pressure value for each wall, the ProSAir model captures the entire spatial and temporal pressure-time history of the walls. To enable a comparison, the ProSAir results are reported as an equivalent uniform

loading by integrating the gauge values across the entire wall. We also report results for a gauge at the wall mid-span for comparison. Both methods presented by Kaplan (1979) are used, namely the "simplistic" method (2-4) and the "detailed" method detailed in Figure 2. Kaplan's results are calculated for two interior reflection cycles, as per the examples in the report. In the following sections, we report on the results of the UFC, Kaplan's simplistic method and ProSAir integrated results across the wall. More detailed results including the Kaplan's detailed method are supplied in Appendix A.

Comparison of side wall loading methods

Figure 11, shows that in six of the eight series the peak pressures of the UFC method are greater than those of the Kaplan's method, which in turn are greater than those of ProSAir for the same external incident pressure. The exceptions are Series 6 and 8 in which Kaplan's method's peak pressure exceeds the UFC's but both still exceed the ProSAir results.

Unsurprisingly therefore, the results for side wall impulse of Figure 12 are similar to the UFC, giving the largest predictions for all except Series 6 and 8.

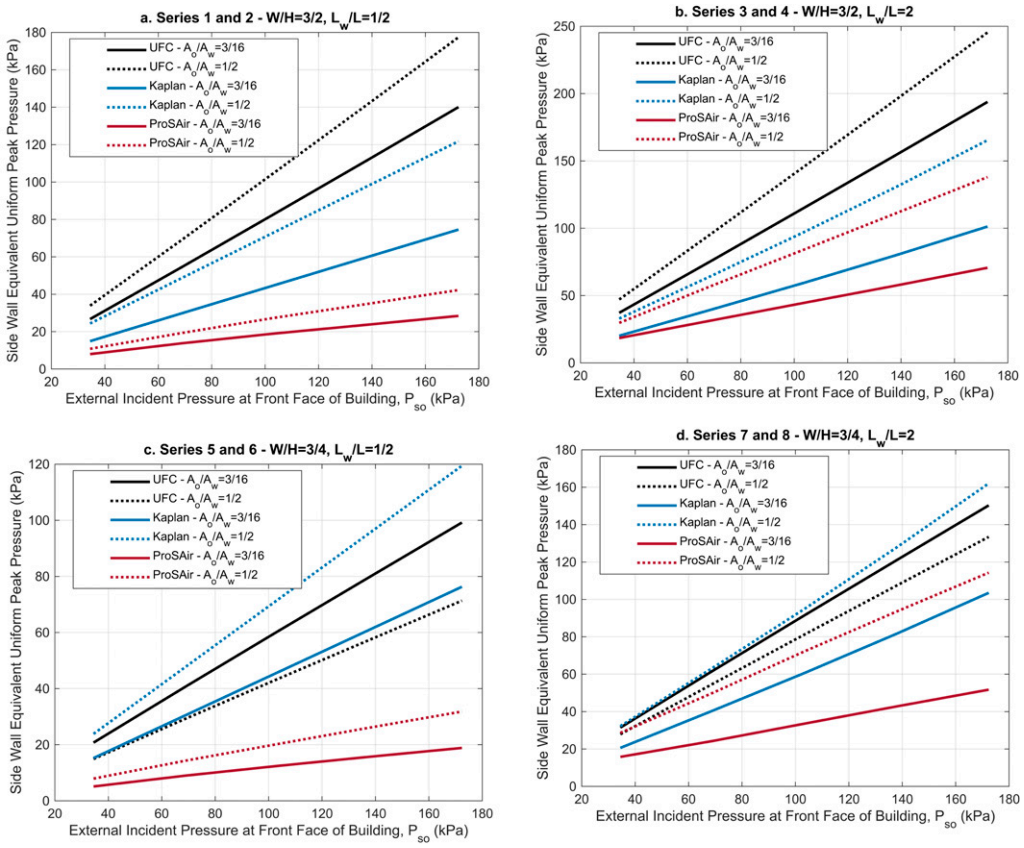


Figure 11. Side wall equivalent uniform peak pressure results for Series 1-8.

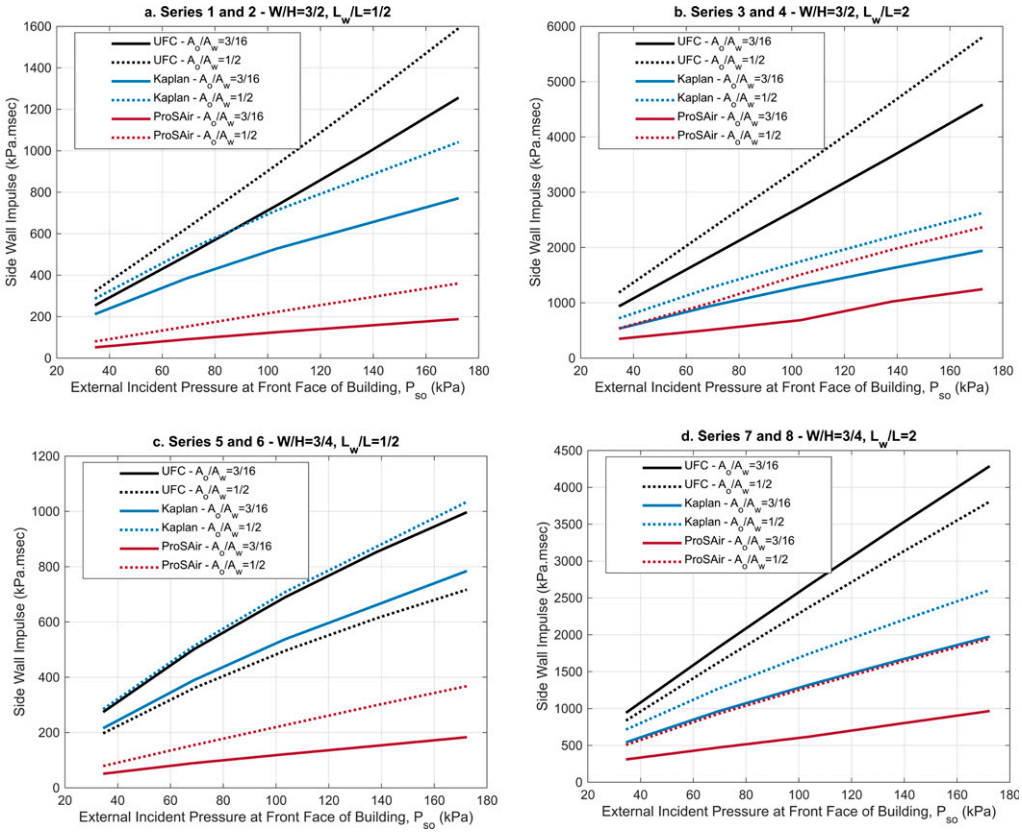


Figure 12. Side wall equivalent uniform first phase impulse results for Series 1-8.

To better quantify the overestimate from the UFC and Kaplan's method we plot the relative results of the UFC and Kaplan divided by those of ProSAir as shown in Figure 13 for pressure and Figure 14 for impulse. As we have confidence in the ProSAir results, Figure 13 shows that the UFC overpredicts the side wall peak pressure by factors of 1.06 to 5.25 and Kaplan's method overpredicts by factors of 1.1 to 4.0. Similarly, Figure 14 shows that the UFC overpredicts the side wall impulse by factors of 1.65 to 6.65 and Kaplan's method by factors of 1.1 to 4.4.

The results can be rearranged to examine the inconsistency shown in Figure 8 for the side wall maximum pressure P_{max} using Equation (3-3) for $W/H = 0.75$. Figure 15 depicts the UFC prediction of Figure 8(b) for Series 2,4,6,8 and 9 with the addition of the ProSAir and Kaplan results. It shows that the rapidly increasing P_{max} with P_{SO} behaviour of the UFC solution for cases of $W/H = \frac{3}{4}$ when using Equation (3-3) is not exhibited by Kaplan's method or ProSAir. Kaplan's results are in good agreement with the UFC solution for $W/H = \frac{3}{4}$ when using Equation (3-2) contrary to the UFC's instructions. ProSAir's also follow the more consistent trend of Equation (3-2) albeit with lower values as previously described. This figure also demonstrates that Kaplan's simplistic method does not reflect the changes with building aspect ratio W/H seen by the UFC and ProSAir, as it predicts identical peak

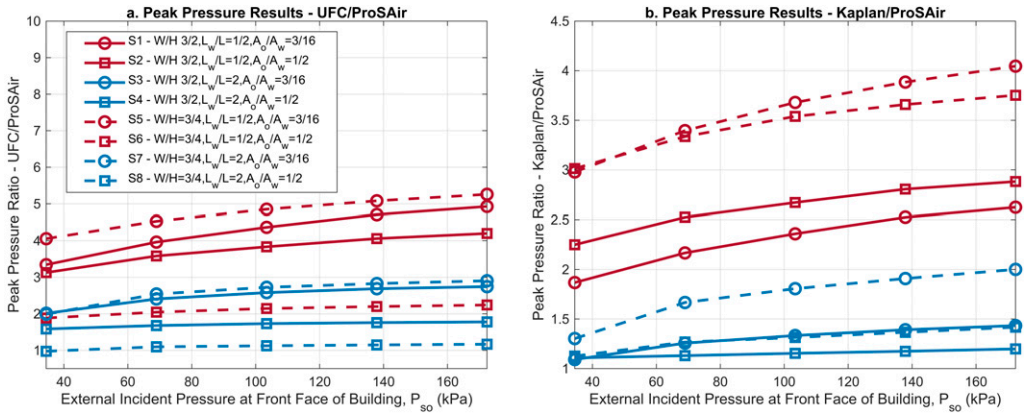


Figure 13. Equivalent uniform peak pressures ratios for Series 1-8; (left) UFC/ProSAir, (right) Kaplan/ProSAir.

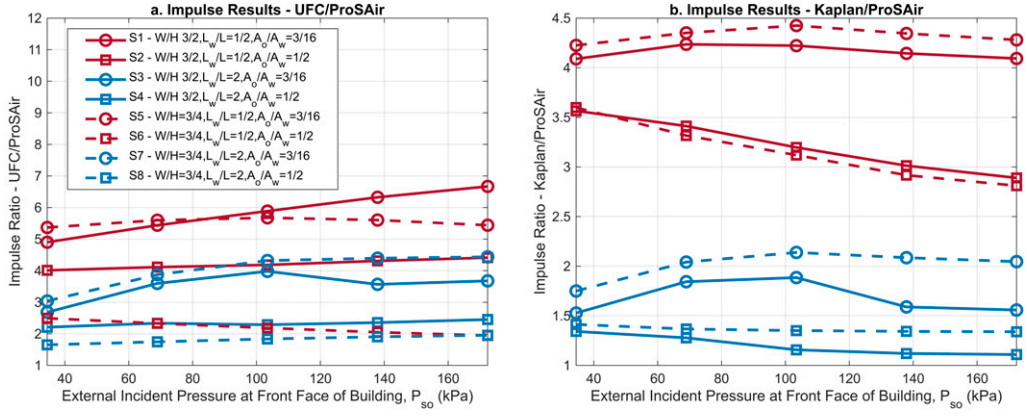


Figure 14. Equivalent uniform impulse ratio for Series 1-8; (left) UFC/ProSAir and (right) Kaplan/ProSAir.

pressure irrespective of the building width. Furthermore, from Figure 11, the UFC predicts higher peak pressure for Series 5 and 7 compared to 6 and 8. This is in contrast to all other series and methods and is an additional demonstration of the inconsistency of Equation (3-3).

To address the issue for the UFC method that the side wall arrival time T_1 is independent of building size for fixed aspect ratio we consider the results for T_1 of Figure 16. The ProSAir results show a strong dependence on the relative opening size A_o/A_w and a far weaker dependence on the shock wave's relative wavelength L_w/L (and hence its incident pressure and shock speed). This inaccuracy in T_1 can contribute to the overprediction of impulse shown in Figure 12.

The question raised about the UFC T_4 behaviour (as demonstrated in Figure 9) can now be examined by comparison with the CFD results of Series 4 and 5, as shown in Figure 17.

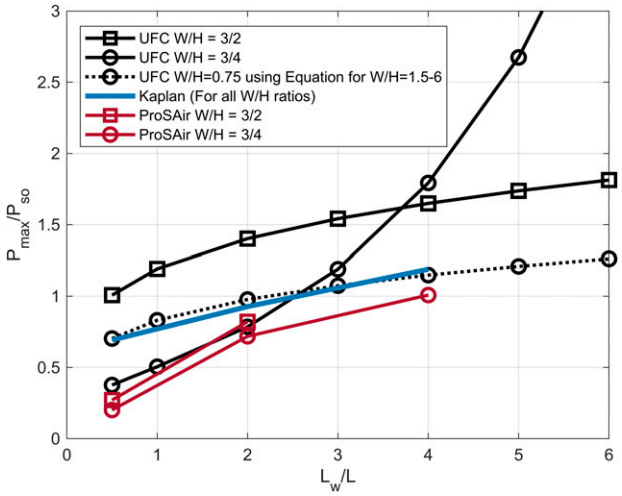


Figure 15. Variation of the UFC side wall P_{max}/P_{SO} with shock relative wavelength L_w/L for $A_o/A_w = 0.5$ and $L/H = 1$.

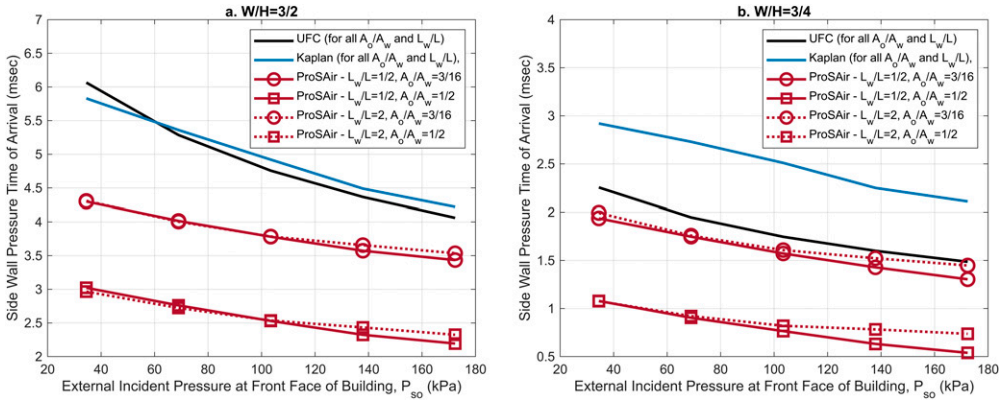


Figure 16. Variation of the side wall time of arrival T_1 with external incident pressure – UFC, Kaplan and ProSAir results; (left) Series 1-4 where $W/H = \frac{3}{4}$ and (right) Series 5-8 where $W/H = \frac{3}{2}$.

Kaplan's solution shows T_4 monotonically decreasing with P_{SO} (with subsequently shock speed U increases). The ProSAir results do not follow a definitive pattern with some indication of a local minimum or point of inflexion in a similar way to the UFC. From examination of the detailed pressure-time histories, this behaviour is due to the inclusion of a relatively small pressure peak in cases 4D and 4E. The UFC and Kaplan assume the load duration is independent of A_o/A_w, while one might expect for a larger opening to expediate the venting of the interior pressure as predicted by the ProSAir results.

The complexity of the loading across the wall can be demonstrated by the ProSAir mid-span gauge as shown in Figure 18. During the UFC's predicted positive load duration, the ProSAir simulation predicts 12 different reflections with the peak pressure suprisingly at the fifth.

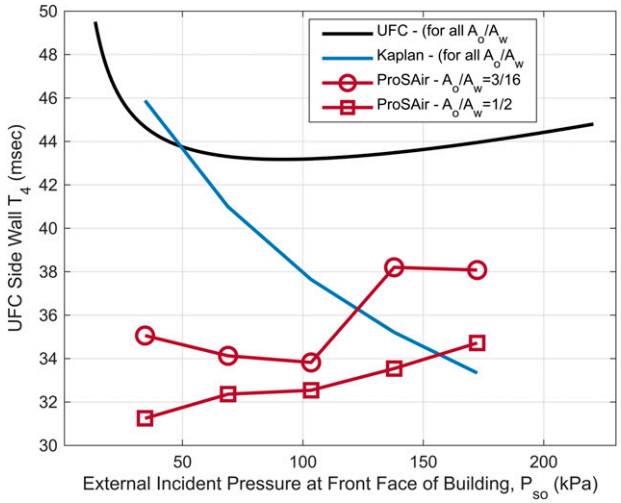


Figure 17. Side wall loading duration T_4 predictions for Series 4-5 where $W/H = 3/4$ and $L_w/L = 2$.

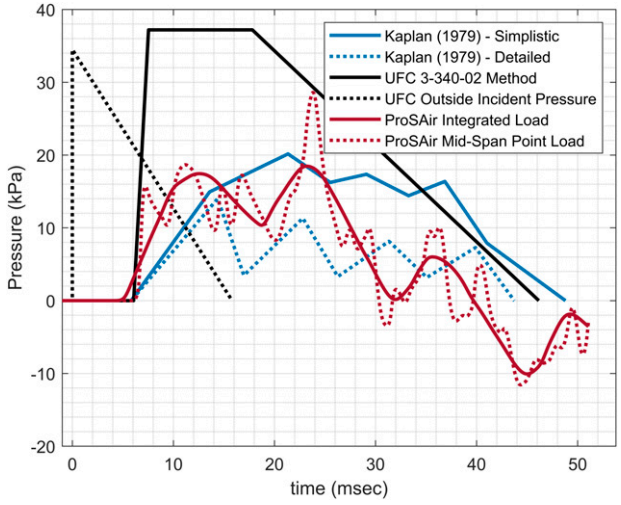


Figure 18. Side wall loadings predictions for Case 3A where $W/H = 3/2$, $A_o/A_w = 3/16$ and $L_w/L = 2$.

This demonstrates the immense challenge the UFC authors faced in accounting for such complex behaviour whilst restricted to a relatively simple mathematical form.

Evaluation of back wall loading methods

The results of the equivalent uniform peak pressure and impulse for the back wall are summarised in Figures 19 and 20, with the detailed pressure-time histories for each case included in Appendix A.

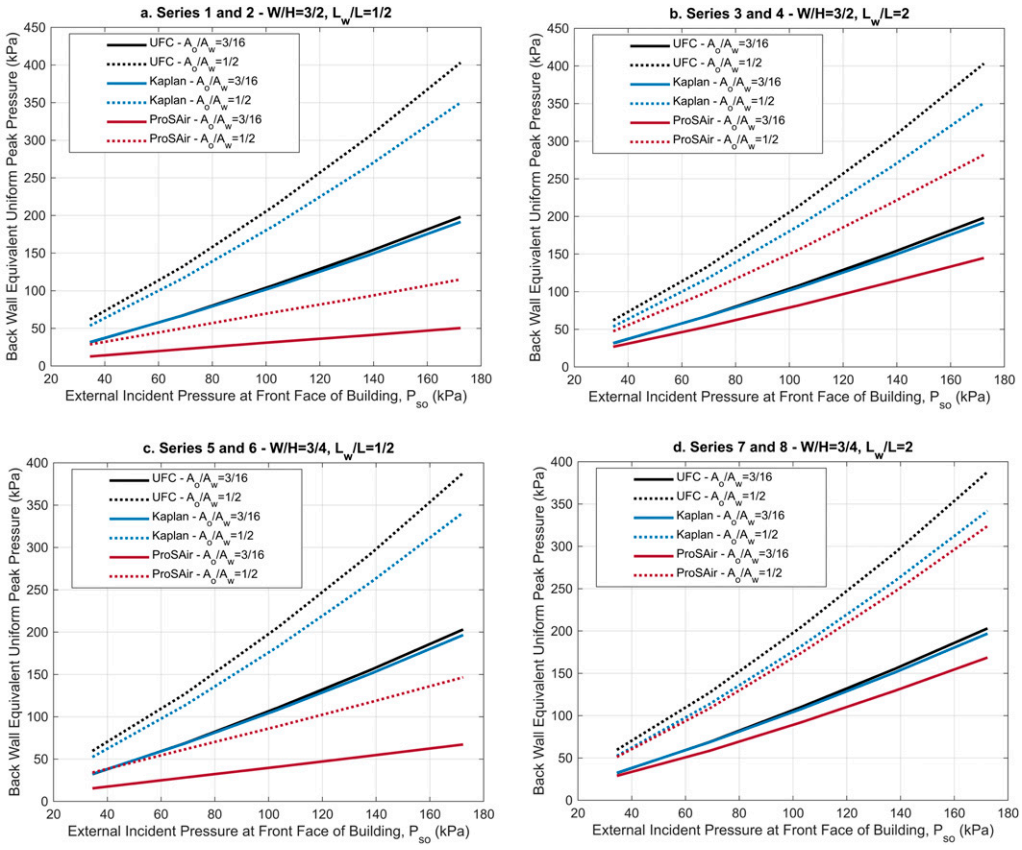


Figure 19. Back wall equivalent uniform peak pressure results for Series 1-8.

The UFC predictions of peak pressure are in good agreement with Kaplan's for all series where $A_o/A_w = \frac{3}{16}$. For series where $A_o/A_w = \frac{1}{2}$ the UFC pressures exceed Kaplan's predictions. ProSAir's pressure results show them both to be significantly overestimated. For the impulse results, we note that Kaplan's method gives a higher estimate than the UFC but both overpredict the impulse compared to ProSAir except for the UFC at small incident pressure. Similarly to the side wall, this can be better quantified by the relative values of the UFC and Kaplan results compared to those of ProSAir as shown in Figure 21 for pressure and Figure 22 for impulse.

The factors across the P_{so} range are less consistent than the side wall. However, we do see factors for the UFC of 1.1 to 3.9 for peak pressure and 0.85 to 1.9 for impulse.

The results for back wall time of arrival T_1 are depicted in Figure 23. The ProSAir results are in good agreement with Kaplan. Both the UFC and Kaplan results are not dependent on A_o/A_w nor L_w/L. The Kaplan and ProSAir results are also not dependent on W/H. While the ProSAir results show a slight dependency on A_o/A_w, it is negligible for design purposes. The UFC results appear to parallel those of Kaplan and ProSAir across the P_{so} range. In Series 6-8 ($W/H = 3/4$) they are consistently delayed by 3.2msec (±5%) and in Series 1-4 ($W/H = 3/2$) by 4.7msec (+/−±4.1%). This consistent delay can be explained by

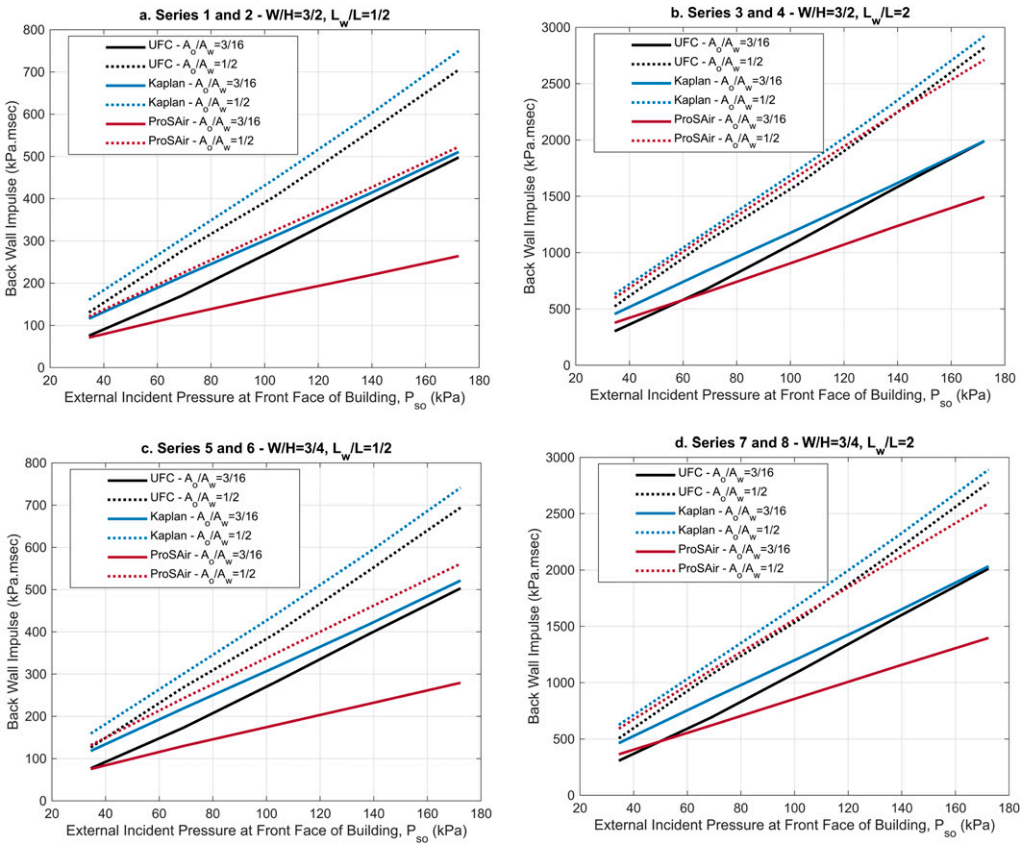


Figure 20. Back wall equivalent uniform first phase impulse results for Series 1-8.

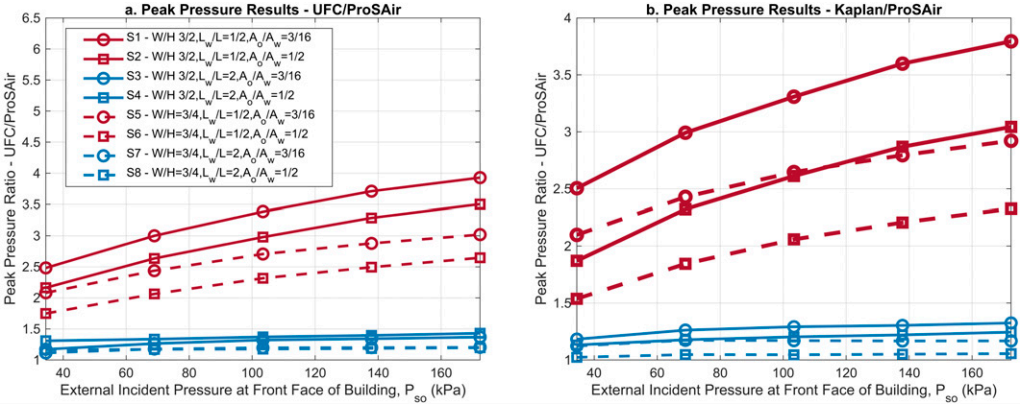


Figure 21. Equivalent uniform peak pressure ratios for Series 1-8; (left) UFC/ProSAir and (right) Kaplan/ProSAir.

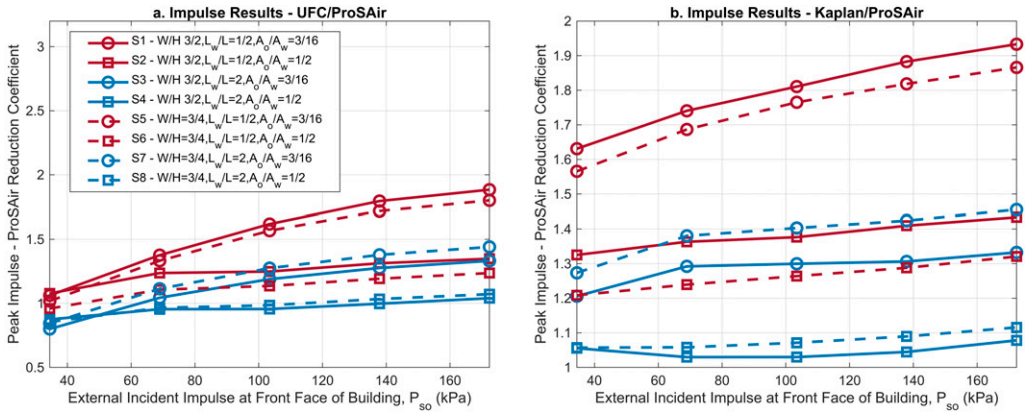


Figure 22. Equivalent uniform impulse ratios for Series 1-8; (left) UFC/ProSAir and (right) Kaplan/ProSAir.

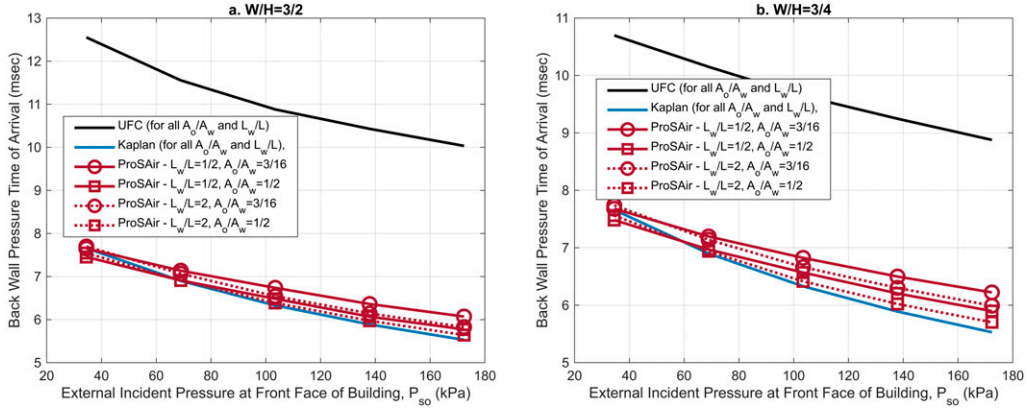


Figure 23. Variation of the predicted back wall time of arrival T_1 with external incident pressure; (left) for Series 1-4 ($W/H = \frac{3}{4}$) and (right) for Series 5-8 ($W/H = \frac{3}{2}$).

ProSAir and Kaplan predicting time T_1' (as per Figure Apx C-1) with the UFC predicting time T_1.

While it appears that ProSAir's impulse predictions are somewhat in agreement with the UFC, it is still unclear if the UFC considers interior re-reflections. The loading on the back wall is composed of a complex set of interior reflections. This can be illustrated by the ProSAir mid-span gauge results in Figure 24. During the ProSAir integrated positive phase, the mid-span gauge records irregularly spaced pressure peaks, with the peak pressure unexpectedly at the fifth.

It is now suggested that the UFC impulse similarity with ProSAir might be coincidental for the cases included in this study. In all cases, ProSAir positive phase duration is longer than the UFC (as depicted in Figure 25), while maintaining a lower peak pressure. The UFC

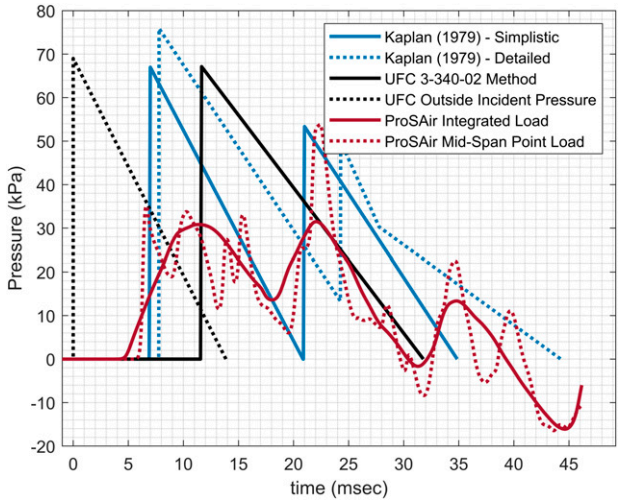


Figure 24. Side wall loadings predictions for Case 3B ($W/H = 3/2$, $A_o/A_w = 3/16$ and $L_w/L = 2$).

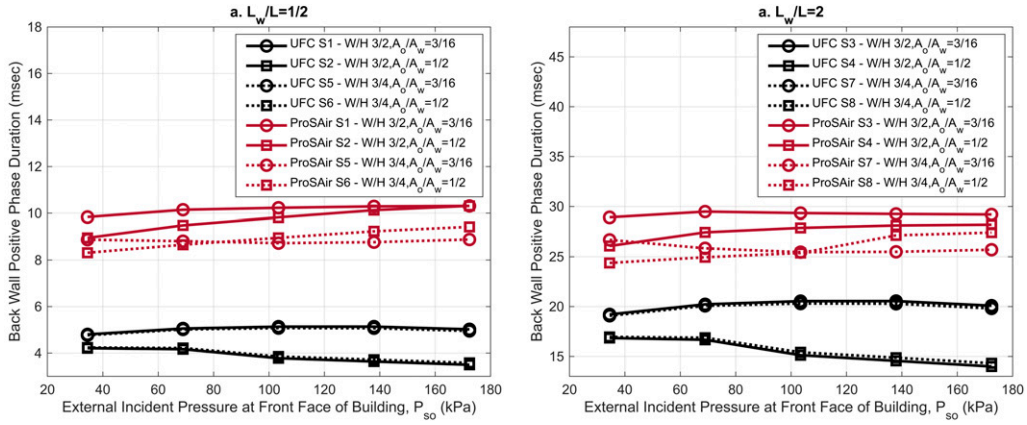


Figure 25. Variation of the predicted back wall positive phase duration with external incident pressure; (left) for Series 1,2,5,6 ($L_w/L = \frac{1}{2}$) and (right) for Series 3,4,7,8 ($L_w/L = 2$).

calculated impulse might be a result of overestimating the pressure for a shorter duration comprised of a single reflection. This requires further investigation which is beyond the scope of this paper.

Conclusions and further work

In this paper we have presented a review of the UFC 3-340-02 (U.S. Department of Defense, 2014) method for predicting the load on interior walls due to ingress of blast pressure through a facade opening. The past research which informed the development of the method has been detailed and contrasted with the final methodology proposed by the UFC. We have explored these differences by conducting a numerical analysis using a modern computational blast loading tool (ProSAir) to

evaluate a series of different structural geometries to elucidate the cumulative effect of the various methods' assumptions.

The UFC provides scant detail of its underlying assumptions and theory for blast ingress, however as a prominent methodology for designing protective structures a reader might fairly assume a well-researched underlying basis informed by relevant experimental data. The critical review of the past research which formed the basis of the UFC methodology highlighted severe shortcomings, many of which were identified by the original authors but are not referenced by the UFC nor evidently accounted for. Both past and present research is severely limited by the lack of high-quality experimental data, with the key publication (Kaplan, 1979) explicitly acknowledging this whilst relying on several unjustified assumptions to account for the shock propagation. The UFC authors were limited to the tools and datasets available at the time of publication; it is concerning that no subsequent revisions of the method have acted on the concerns and recommendations in Kaplan's original publication (Kaplan, 1979) nor attempted to use modern tools to evaluate these assumptions.

In our numerical study using modern computational tools a stark contrast is visible between the pressure predictions for the different methods. The UFC results are seen to greatly exceed the side wall loadings predicted by ProSAir, with pressures and impulses of up to 425% and 565% respectively relative to ProSAir. The ProSAir results demonstrated that parameters such as the shock time of arrival are dependent on the physical dimensions of the structure rather than the dimensionless geometric ratios assumed in the UFC.

By contrast, the differences in the back wall loading predictions are less dramatic. Whilst the UFC peak pressures were again consistently higher than the ProSAir predictions by up to 290%, surprisingly the impulse predictions were similar. From examination of the detailed pressure-time results, it is theorised that this similarity is coincidental. It was observed that the UFC predicts higher peak pressures than ProSAir but for a shorter duration. It is hypothesised that the UFC methodology only accounts for a single reflection of higher peak pressure and shorter duration, for which the impulse is coincidently similar to ProSAir (which accounts for all the interior re-reflections). This will be examined in future work by the authors as a greater variation in structural geometries is required to ascertain the relation.

The considerable overestimates of the loadings by the UFC methodology, relative to modern modelling techniques, could results in significant overdesign of protective structures greatly increasing costs and environmental impacts. Furthermore, it may even result in structures foregoing protection where indicative costs based on UFC predictions are too prohibitive.

Whilst the numerical study presented here included 45 different loading cases, considerably more simulations are required to fully evaluate the accuracy of the UFC across its stated range of applicability. Similarly, the absence of high-quality experimental data of blast ingress is an immediate lacuna that needs filling to form the basis for any approach seeking to update or replace the UFC methodology. In the interim, the use of CFD simulations to evaluate the interior loading due to pressure ingress is recommended for a more realistically estimated blast loadings, particularly for the side walls of structures.

As part of the future work identified by the authors in the course of this review paper, work on validating ProSAir specifically against pressure ingress scenarios has been conducted and yet unpublished. Furthermore, this modelling approach has been extended to simulate 720 case studies to encapsulate the full range of structures and blast parameters considered in the UFC. This exhaustive study (paper in preparation) will be used to justify an improved method for predicting blast ingress, which in contrast to the UFC will include complete transparency of the underlying data and assumptions.

Declaration of Conflicting Interests

The author(s) declared no potential conflicts of interest with respect to the research, authorship, and/or publication of this article.

Funding

The author(s) received no financial support for the research, authorship, and/or publication of this article.

ORCID iDs

Alex Eytan https://orcid.org/0000-0002-0767-6551
Shaun A Forth https://orcid.org/0000-0002-2401-6125
Erik G Pickering https://orcid.org/0000-0002-5248-9296
Stephanie J Burrows https://orcid.org/0000-0002-8202-9020

Supplemental Material

Supplemental material for this article is available online.

References

Abdelalim O (2013) *Blast Hazard Mitigation through Vented Suppressive Shields, PhD Thesis*. Ottawa, Canada: Carleton University.

ASCE 59-11 (2011) *Blast protection of buildings*. USA: American Society of Civil Engineers.

Ayvazyan H, Dede M, Dobbs N, et al. (1986) *Structures to Resist the Effects of Accidental Explosions Volume II, Blast, Fragment, and Shock Loads (ARLCD-SP-84001)*. USA: U.S. Army Armament Research, Development and Engineering Center.

Berger S, Ben-Dor G and Sadot O (2015) Experimental and numerical investigations of shock-wave attenuation by geometrical means: a single barrier configuration. *European Journal of Mechanics - B: Fluids* 50: 60–70. DOI: 10.1016/j.euromechflu.2014.11.006.

Britan A, Igra O, Ben-Dor G, et al. (2006) Shock wave attenuation by grids and orifice plates. *Shock Waves* 16(1): 1–15. DOI: 10.1007/s00193-006-0019-0.

BRL (1962) *Information Summary of Blast Patterns in Tunnels and Chambers*. 2nd edn. *Aberdeen Proving Ground MD: Ballistic Research Laboratories, Aberdeen Proving Ground*. Memorandum Report No. 1390.

Brode HL (1957) A calculation of the blast wave from a spherical charge of TNT. In: *U.S. Air Force Project Rand, Research Memorandum RM-1965*.

Codina R and Ambrosini D (2018) Full-scale testing of leakage of blast waves inside a partially vented room exposed to external air blast loading. *Shock Waves* 28(2): 227–241. DOI: 10.1007/s00193-017-0733-9.

Codina R and Ambrosini D (2019) Numerical and analytical study of overpressures and impulses inside a masonry box subjected to external blast loading. *International Journal of Protective Structures* 10(3): 270–288. DOI: 10.1177/2041419619843636.

Coulter GA (1968) Air shock filling of model rooms. In: *U.S. Army Material Command, Ballistic Research Laboratories. Memorandum Report No.: 1916*.

Coulter GA (1969) Air shock and flow in model rooms. In: *Ballistic Research Laboratories, Aberdeen Proving Ground. Memorandum Report No.: 1987*.

CSA S850-12 (2012) *Design and Assessment of Buildings Subjected to Blast Loads*. Canada: Canadian Standards Association.

Dib N, Zéhil GP and Rigby S (2022) On the blast-wave shielding effect of porous buildings. *Journal of Fluids and Structures* 115. DOI: 10.1016/j.jfluidstructs.2022.103787.

Drazin W (2017) *Blast Propagation and Damage in Urban Topographies, PhD Thesis*. Cambridge, United Kingdom: University of Cambridge.

Feldgun VR, Karinski YS, Edri I, et al. (2016) Prediction of the quasi-static pressure in confined and partially confined explosions and its application to blast response simulation of flexible structures. *International Journal of Impact Engineering* 90: 46–60. DOI: 10.1016/j.ijimpeng.2015.12.001.

Forth S (2022) ProSAir 2022.11 user guide. In: *Cranfield Defence and Security, Applied Mathematics and Scientific Computing*.

Friedlander FG (1946) The diffraction of sound pulses I. Diffraction by a semi-infinite plane. *Proceedings of the Royal Society A* 186(1006). DOI: 10.1098/rspa.1946.0046.

Glasstone S (1964) *The Effects of Nuclear Weapons*. 2nd ed. USA: U.S. Atomic Energy Commission.

Idf HFC (2010) Israeli civil defence regulations (specifications for building shelters). In: *Israel Defence Forces, Home Front Command*.

Kaplan K (1979) *Accidental Explosions and Effect of Blast Leakage into Structures*. USA: U.S. Army Armament Research and Development Command.

Kingery C and Watson G (1982) *Blast leakage into hardened aircraft shelter models, Technical Report ARBRL-TR-02392*. USA: US Army Ballistics Research Laboratory.

Mercx WPM (1990a) *Pressure Development in a Chamber Due to an Entering Shock Wave, TNO-report PML 1990-C1*. Rijswijk, The Netherlands: TNO.

Mercx WPM (1990b). Pressure Development in a Chamber due to an Entering Shock Wave, Part Two: Influence of Window Panes, TNO-report *PML* 1990-C122. Rijswijk, The Netherlands: TNO.

Mercx WPM (1991) *Pressure Development in a Chamber Due to an Entering Shock Wave, Part Three: Variation of Chamber Depth and Final Results, TNO-report PML 1991-C34.* Rijswijk, The Netherlands: TNO.

Ram O, Nof E and Sadot O (2016) Dependence of the blast load penetrating into a structure on initial conditions and internal geometry. *Experimental Thermal and Fluid Science* 78: 65–74. DOI: 10.1016/J.EXPTHERMFLUSCI.2016.05.012.

Singapore Civil Defence Shelter Act (1997) *Singapore Ministry of Home Affairs*. Singapore: Singapore Civil Defence Shelter Act.

Skews B (2005) Shock wave interaction with porous plates. *Experiments in Fluids* 39(5): 875–884. DOI: 10.1007/s00348-005-0023-7.

Smith PD, Rose TA, Krahe SL, et al. (2002) *Façade Failure Effects on Blast Propagation along City Streets*. Proceedings of the Institution of Civil Engineers, Structures & Buildings 156, SB4, 359–365, 13003.

U.S. Army Corps of Engineers (2009) *UFGS 23-33-56 Self-Acting Blast Valves*. USA: U.S. Army Corps of Engineers.

US Department of Commerce. (1969). Structures to Resist the Effects of Accidental Explosions (TM 5-1300, NAVFAC P-397, AFM 88-22). In: *U.S. Department of Commerce, National Technical Information Service*.

U.S. Department of Defense (1990) *Structures to Resist the Effects of Accidental Explosions - Revision 1 (TM 5-1300)*. USA: U.S. Department of Defense.

U.S. Department of Defense (2014) Unified Facilities Criteria (UFC) - Structures to Resist the Effects of Accidental Explosions. In: *U.S. Army Corps of Engineers, Naval Facilities Engineering Command, Air Force Civil Engineer Support Agency.*

U.S. FEMA (2006) *Design Guidance for Shelters and Safe Rooms - FEMA 453*. U.S. Department of Homeland Security.

Wilton C, Kaplan BL and Gabrielsen BL (1978) The shock tunnel - history and results - volume II. In: *Defense Civil Preparedness Agency, Summary Report 7618-1*.

Xu W, Wu W and Lin Y (2018) Numerical method and simplified analytical model for predicting the blast load in a partially confined chamber. *Computers and Mathematics with Applications* 76(2): 284–314. DOI: 10.1016/j.camwa.2018.04.019.



https://dspace.org/

Blast wave ingress into a room through an opening – review of past research and US DoD UFC 3-340-02

Eytan, Alex; Forth, Shaun A.; Pickering, Erik G.; Hazael, Rachael; Burrows, Stephanie J.

2025-09
Sage
https://doi.org/10.1177/20414196241277222
Eytan A, Forth SA, Pickering EG, et al., (2025) Blast wave ingress into a room through an opening – review of past research and US DoD UFC 3-340-02. International Journal of Protective Structures, Volume 16, Issue 3, September 2025, pp. 799-822

Downloaded from a DSpace repository. https://dspace.org/